remote sensing

MDPI

Supplementary information

Evidence of widespread volcanic activity near Hebrus Valles on Mars revealed by SHARAD

Stefano Nerozzi [1,*], Michael S. Christoffersen [2], John W. Holt [1], Christopher W. Hamilton [1]

1. Notes on the SHARAD power spectrum

The chirp power spectrum radiated by SHARAD is known to be non-uniform with as much as 3.5 dB variability [1] (Fig. S1). As described in section 2.2.3, we take this aspect into account by iterating the loss tangent inversion methods across the entire SHARAD chirp bandwidth and by applying a weighted average. We calculate the weights by normalizing the calibrated SHARAD linear power spectrum from the PDS, as shown in Fig. S2 below.

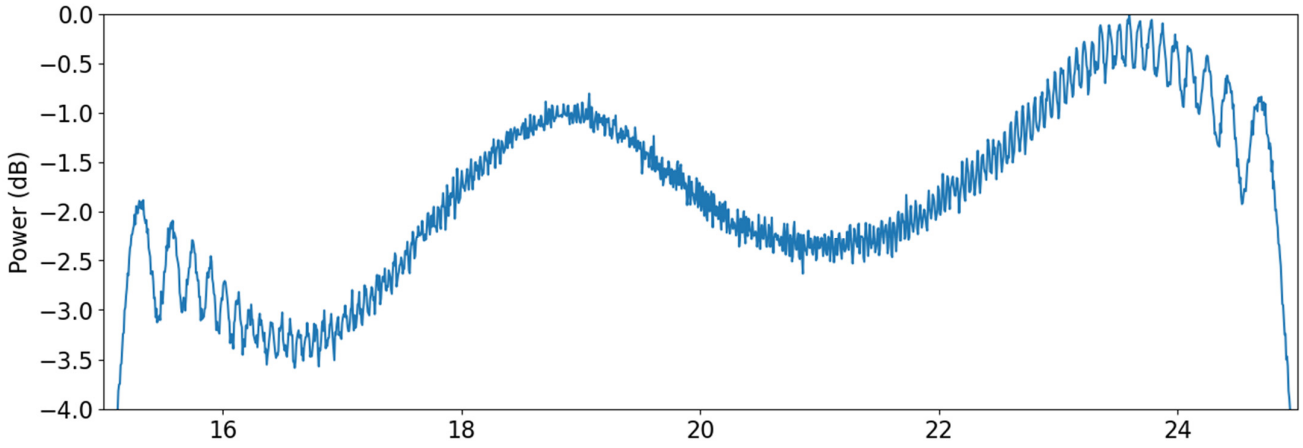

Figure S1: Power spectrum of the chirp pulse radiated by SHARAD. The maximum power is set at 0 dB. The source of this spectrum is "reference_chirp_p20tx_p00rx.dat" from the PDS.

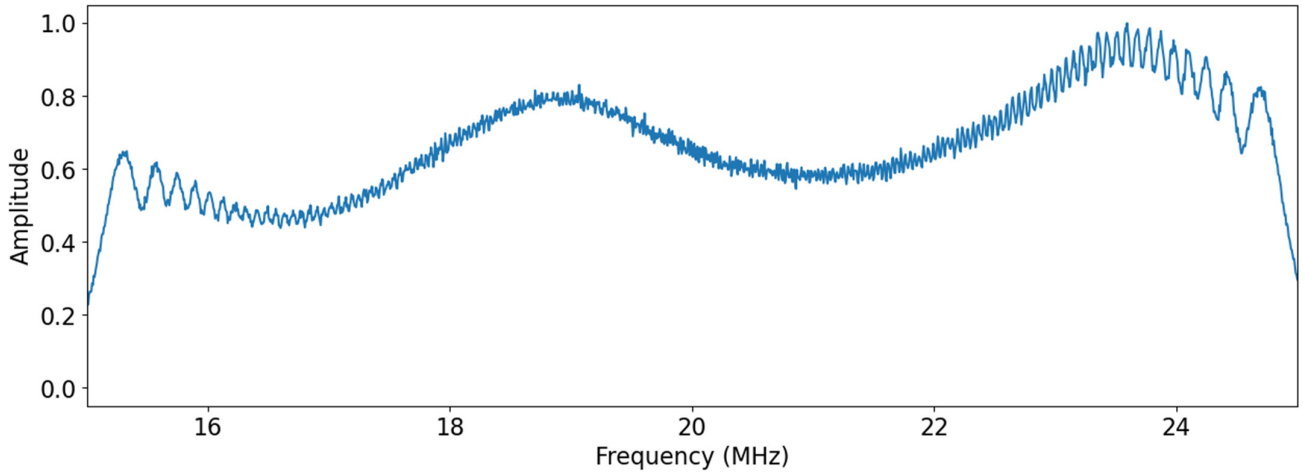

Figure S2: Normalized amplitude spectrum of the chirp pulse radiated by SHARAD. The source of this spectrum is "refer-ence_chirp_p20tx_p00rx.dat" from the PDS.

2. Granicus Valles subregion loss tangent results

Below we report the loss tangent results from both methods described in the main article [2,3] for each subregion (A to P) in Granicus Valles. Note that the results of the *power loss vs. time delay* method for region P yields an unphysical negative loss tangent; we report this result for completeness.

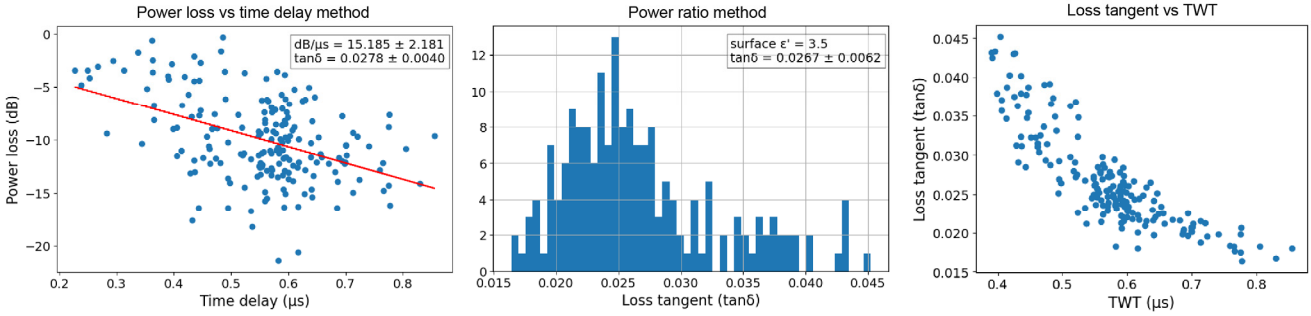

Figure S3: Loss tangent results for subregion A.

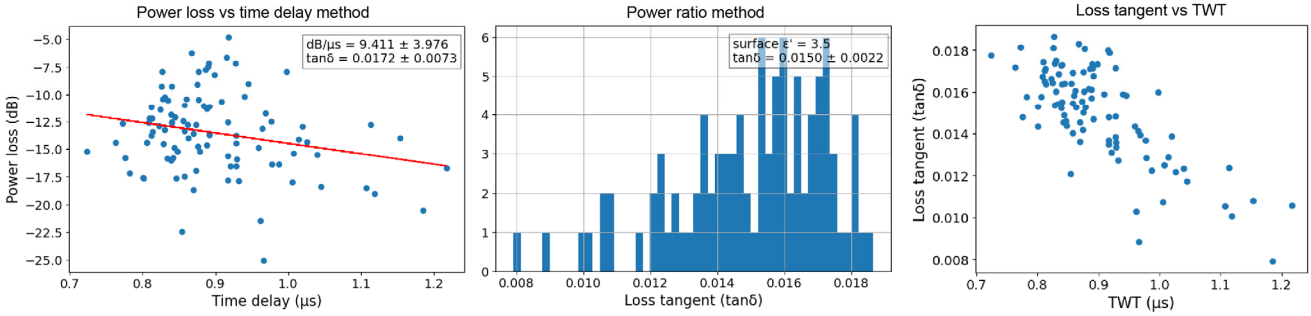

Figure S4: Loss tangent results for subregion B.

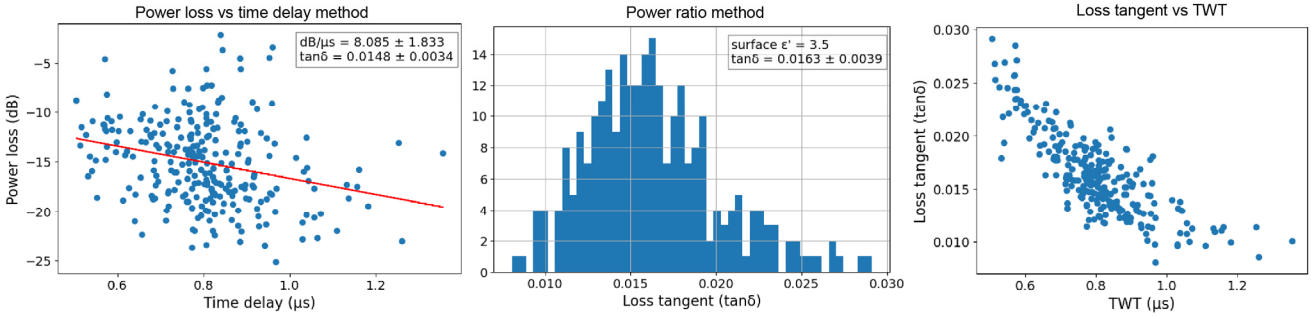

Figure S5: Loss tangent results for subregion C.

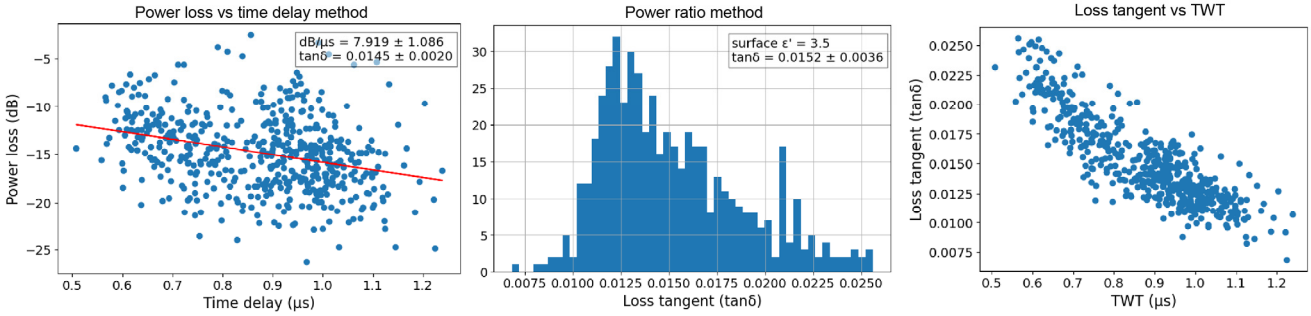

Figure S6: Loss tangent results for subregion D.

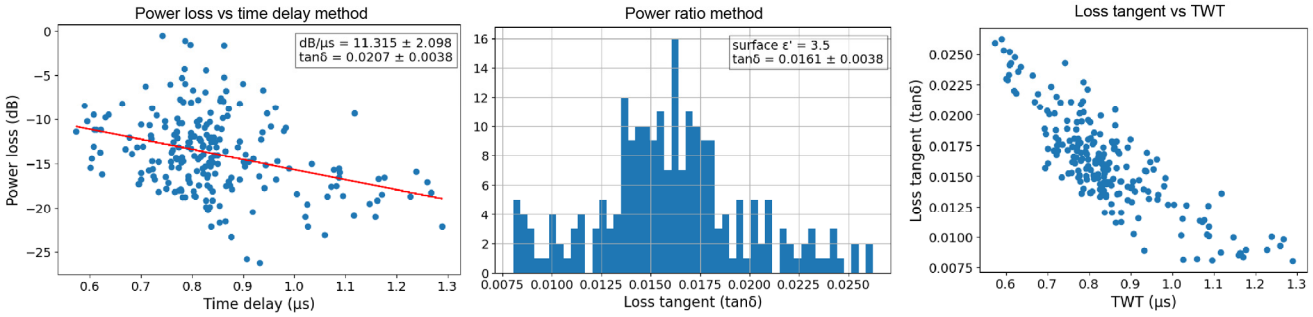

Figure S7: Loss tangent results for subregion E.

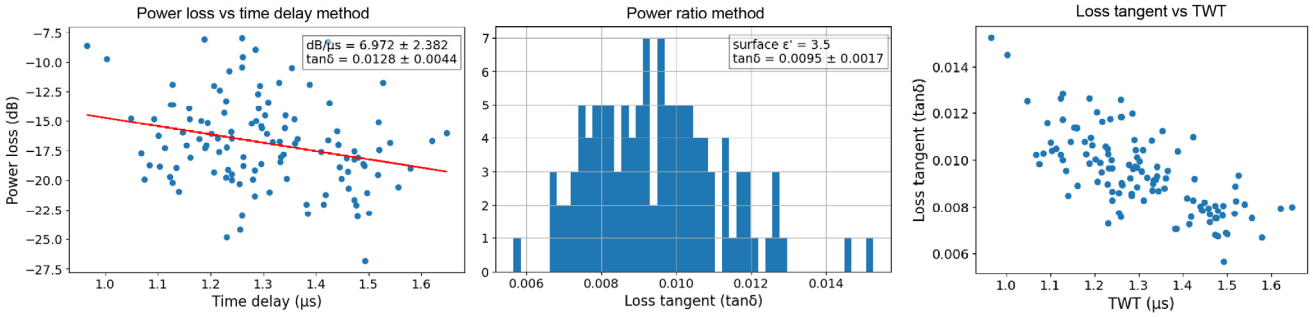

Figure S8: Loss tangent results for subregion F.

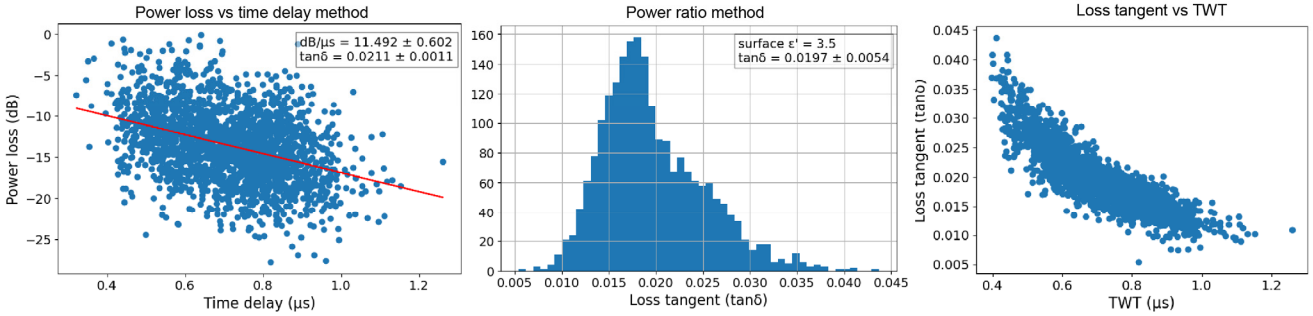

Figure S9: Loss tangent results for subregion G.

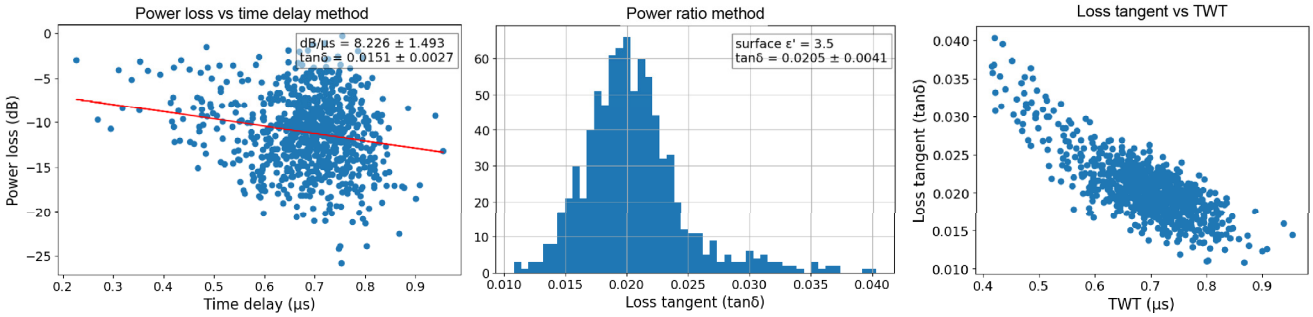

Figure S10: Loss tangent results for subregion H.

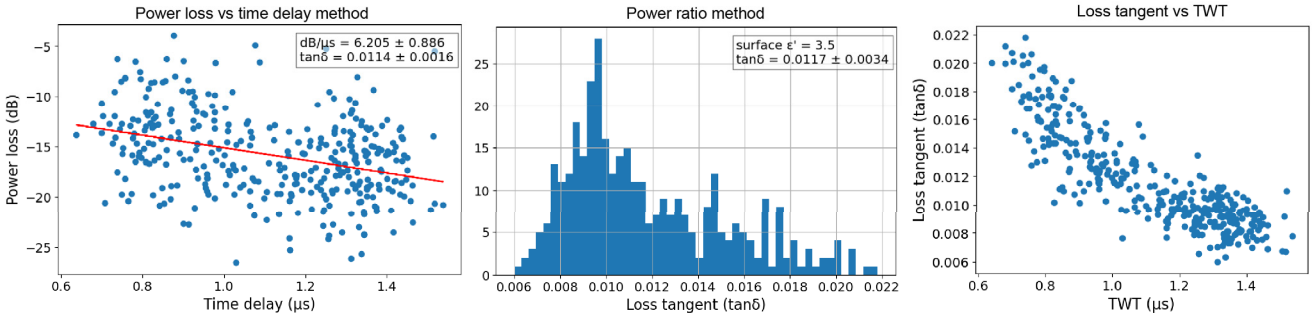

Figure S11: Loss tangent results for subregion I.

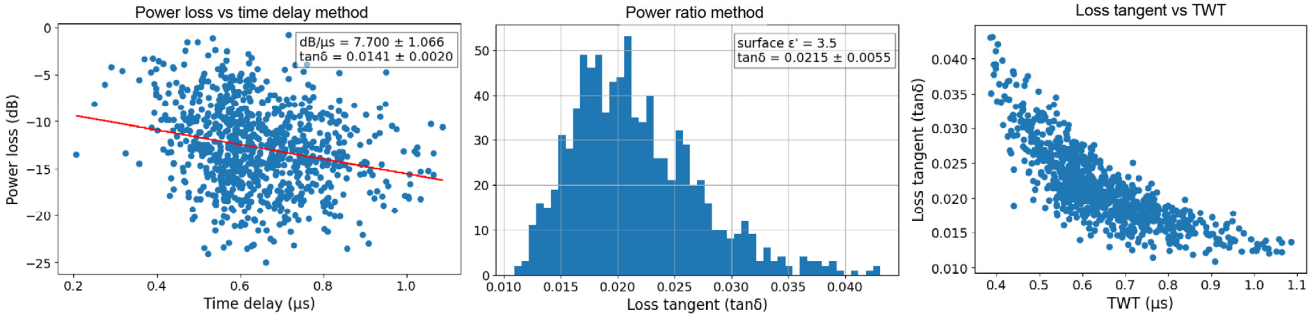

Figure S12: Loss tangent results for subregion J.

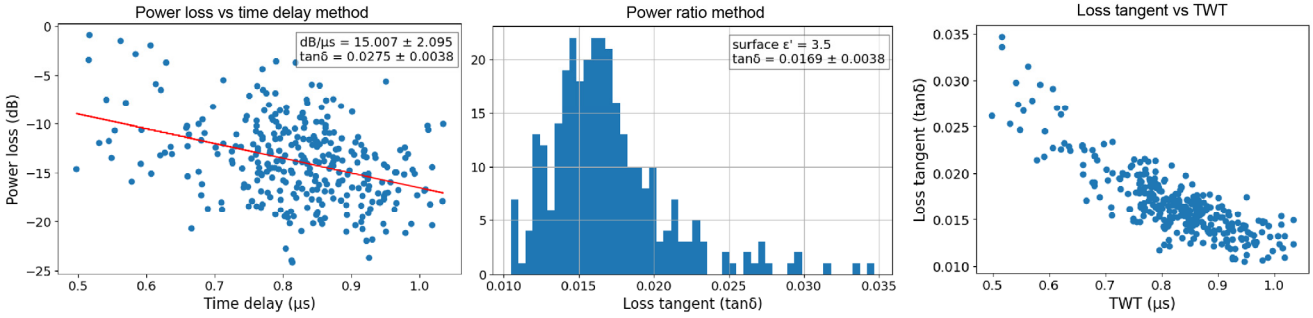

Figure S13: Loss tangent results for subregion K.

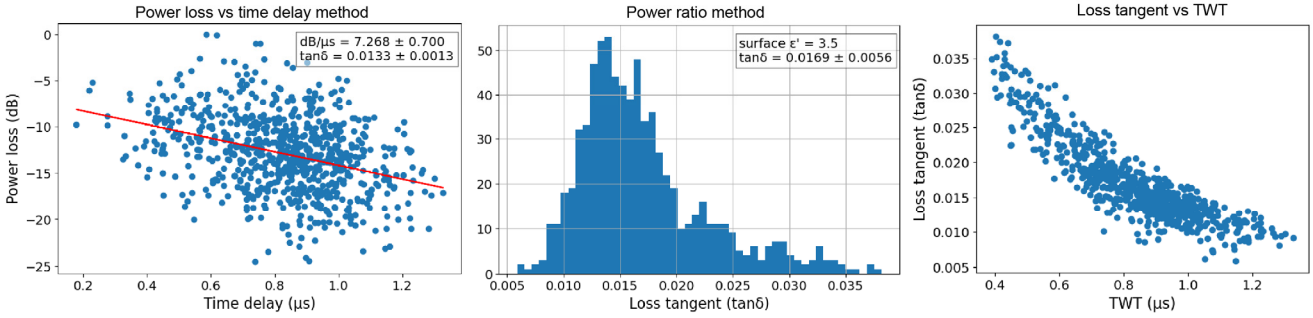

Figure S14: Loss tangent results for subregion L.

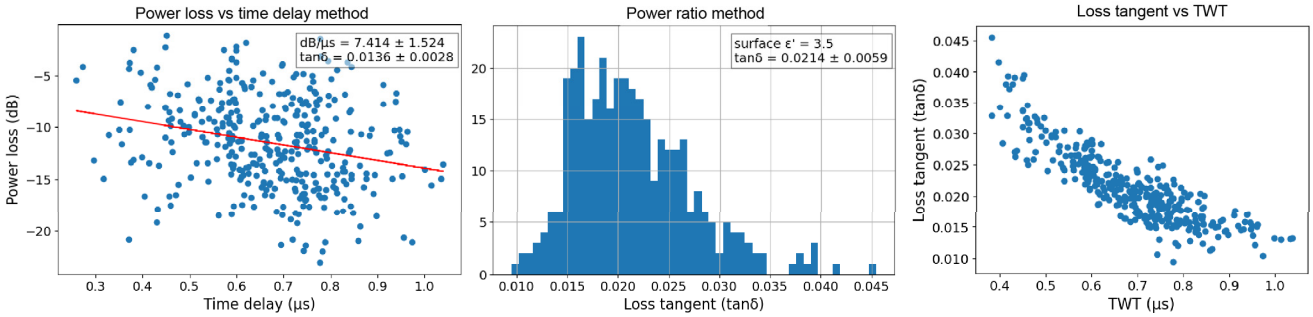

Figure S15: Loss tangent results for subregion M.

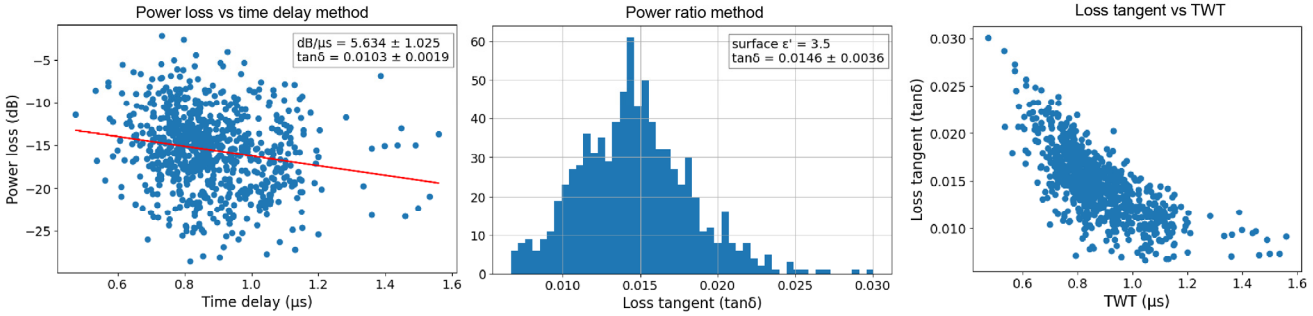

Figure S16: Loss tangent results for subregion N.

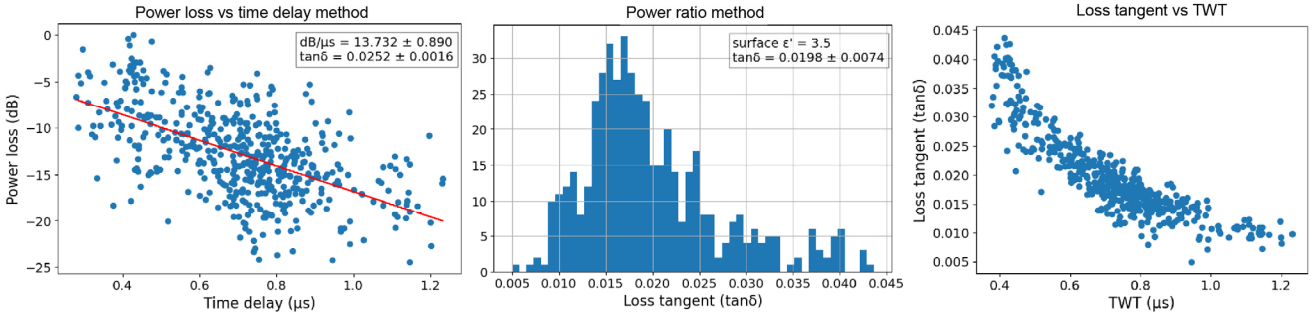

Figure S17: Loss tangent results for subregion O.

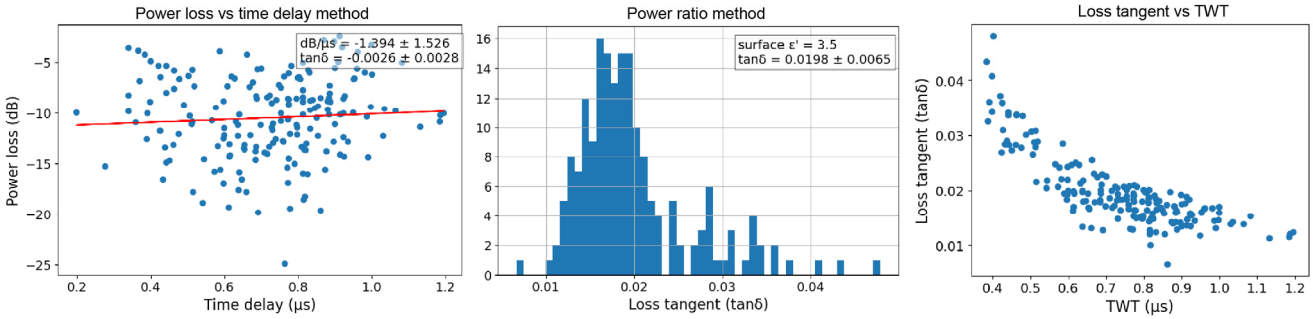

Figure S18: Loss tangent results for subregion P.

References

1. Campbell, B.A.; Morgan, G.A. Fine-Scale Layering of Mars Polar Deposits and Signatures of Ice Content in Nonpolar Material From Multiband SHARAD Data Processing. *Geophysical Research Letters* **2018**, *45*, 1759–1766, doi:10.1002/2017GL075844.
2. Campbell, B.; Carter, L.; Phillips, R.; Plaut, J.; Putzig, N.; Safaeinili, A.; Seu, R.; Biccari, D.; Egan, A.; Orosei, R. SHARAD Radar Sounding of the Vastitas Borealis Formation in Amazonis Planitia. *J. Geophys. Res.* **2008**, *113*, E12010, doi:10.1029/2008JE003177.
3. Grima, C.; Kofman, W.; Mouginot, J.; Phillips, R.J.; Hérique, A.; Biccari, D.; Seu, R.; Cutigni, M. North Polar Deposits of Mars: Extreme Purity of the Water Ice. *Geophysical Research Letters* **2009**, *36*, L03203, doi:10.1029/2008GL036326.